High-Throughput Visual MIMO Systems for Screen-Camera Communications

Fujihashi, Takuya; Koike-Akino, Toshiaki; Orlik, Philip V.; Watanabe, Takashi

Abstract

Screen-camera communications, using a liquid crystal display (LCD) screen and camera image sensors, have been attractive variants of visible light communications (VLC) since any external light-emitting modules and photo detectors are required for recent mobile devices, which are usually equipped with display and camera. A major issue in screen-camera communications is a performance loss in transmission rate due to nonlinear channel impairments with ambient noise. To improve transmission rates, we investigate the impact of nonlinear channel equalization, nonbinary channel coding, probabilistic shaping, and nonlinear precoding for high-order modulation schemes. Experimental evaluations using an LCD screen and camera demonstrate that our proposed scheme achieves 3.8–3.3 times higher transmission rates compared to existing schemes for a communication distance of 60–160 cm.

High-Throughput Visual MIMO Systems for Screen-Camera Communications

Takuya Fujihashi, *Member, IEEE,* Toshiaki Koike-Akino, *Senior Member, IEEE,*
Philip V. Orlik, *Senior Member, IEEE,* and Takashi Watanabe, *Member, IEEE*

Abstract—Screen-camera communications, using a liquid crystal display (LCD) screen and camera image sensors, have been attractive variants of visible light communications (VLC) since any external light-emitting modules and photo detectors are required for recent mobile devices, which are usually equipped with display and camera. A major issue in screen-camera communications is a performance loss in transmission rate due to nonlinear channel impairments with ambient noise. To improve transmission rates, we investigate the impact of nonlinear channel equalization, nonbinary channel coding, probabilistic shaping, and nonlinear precoding for high-order modulation schemes. Experimental evaluations using an LCD screen and camera demonstrate that our proposed scheme achieves 3.8–3.3 times higher transmission rates compared to existing schemes for a communication distance of 60–160 cm.

Index Terms—visible light communications, MIMO, screen-camera transmission, nonlinear equalization, nonbinary coding, lattice precoding, probabilistic shaping.

I. Introduction

Visible light communications (VLC) [1]–[3] have emerged as promising complementary technologies to conventional radio-frequency (RF) wireless communications. Screen-camera communications [4]–[7] are such VLC technologies, where digital data can be transmitted via image signals from a screen to a camera. For screen-camera communications, digital bits are encoded in the screen image on devices, e.g., laptop computers and smart phones. A receiver equipped with camera image sensors captures the screen to decode the information. Screen-camera communications can be used for various wireless applications, such as inter/intra vehicle communications [8], near field communications [9], [10], and augmented reality [11]. The use of screen and camera can form so-called multi-input multi-output (MIMO) systems in which optical transmissions by an array of light-emitting devices are received by an array of photo-detector elements. Although typical frame rates of screen and camera devices are relatively low in general (e.g., 50 frames per second), high-definition screen and camera can realize massive spatial multiplexing gain to transfer a large amount of information bits at once.

A major challenge of the screen-camera communications is to increase the transmission rate in nonlinear channels with ambient noise. In particular, there are three issues in such links as follows. First, an encoded image on the screen is distorted due to receiver's perspective. When the receiver captures the encoded image on a rectangular screen from a certain angle, the captured image will become a trapezoid. This phenomenon is referred to as perspective distortion [12]. Second, the luminance of encoded image is impaired by ambient lights. This impairment causes errors in the encoded information, resulting in a low transmission rate. Third, the spectrum sensitivity of red, green, and blue channels on the camera sensor is non-orthogonal and highly nonlinear. Specifically, the output of one color channel may be degraded by the intensity of the other color channels. This is known as color mixing.

To overcome the above-mentioned issues, some approaches [13]–[17] have been proposed for screen-camera links to improve the transmission rates. For example, PixNet [13] uses orthogonal discrete multi-tone (DMT) for single-color channel transmission. In PixNet, the perspective distortion and ambient lights are also mitigated. Another approach in [14] discusses the effect of high-order modulation for the communications with single color channel. In addition, some approaches [15], [17] use three color channels, i.e., red, green, and blue, to improve the transmission rate. However, the increase of transmission rates are still marginal due to nonlinearity.

To increase the transmission rate in screen-camera communications, we propose a visual MIMO system exploiting three color channels and multilevel modulation. In this case, we need to 1) improve bit reliability at each constellation having non-identical noise variance and 2) mitigate channel distortion due to pixel and color mixing. To this end, we introduce four state-of-the-art techniques in the proposed scheme. First technique is the use of channel equalizations [18] based on minimum mean-square error (MMSE) and nonlinear Volterra series [19]–[21], which have been well-studied in nonlinear amplifiers for wireless communications and nonlinear fibers for optical communications. The channel equalization is used to revert back the color/pixel-mixing to retrieve transmitted constellations by minimizing the mean squared error between the desired constellation and equalized signal. As screen and camera devices may have undesired nonlinear response, we also consider Volterra series expansion to reduce such nonlinear channel effects. Although how to design linear channel equalization in VLC was discussed in [22], there was no comparative evaluation of the throughput improvement in screen-camera communications. Second technique is the use of channel coding based on nonbinary low-density parity-check (LDPC) codes [23]–[27]. The nonbinary

LDPC codes are designed in high-order Galois Fields to encode multiple bits at once into a multilevel modulation symbol. For wireless [25] and optical communications [24], nonbinary codes have been verified to improve the reliability of communications using multilevel modulation formats. To accomplish high transmission rate in screen-camera communications, we introduce the nonbinary coding together with high-order modulation schemes. Third technique is nonlinear precoding, called vector perturbation (VP) [28]–[30]. The VP can resolve the color/pixel mixing effect prior to transmission in addition to reduce noise enhancement due to the channel inversion by using the lattice perturbation vector. In some wireless and optical communications systems, a receiver periodically sends back a feedback of channel state information for precoding operations to adapt the channel conditions. This study is the first to evaluate an impact of precoding techniques supposed that the transmitter have a knowledge of channel state information prior to transmission. Forth technique is probabilistic shaping [31], [32] which manipulates the signal constellation via non-uniform probability of the occurrence. The probabilistic shaping has been used to compensate for the theoretical shaping gap of regular quadrature-amplitude modulation (QAM) formats over an idealistic Gaussian-like signal distribution [33]. This study is the first to introduce the probabilistic shaping in the screen-camera communications to exploit the shaping gain in the presence of non-identical noise variance at each constellation due to nonlinearity. By integrating those techniques to improve reliability and to mitigate the channel distortions, we demonstrate that the proposed scheme can increase the transmission rates, up to 3.8 times higher than existing studies, under experimental measurements with a general-purpose screen and camera sensor.

In [34], we have reported a preliminary analysis on screen-camera communications using high-order modulation and non-linear equalization. In this paper, we extend the proposed scheme by introducing probabilistic shaping and nonlinear precoding techniques to further improve the transmission rates. Although these techniques are studied extensively in wireless and fiber-optic communications systems, there are no studies showing benefits of these techniques in screen-camera VLC systems. From experimental analysis, it is found that nonlinear precoding can maintain higher transmission rates in longer communication distances. In addition, probabilistic shaping can yield higher transmission rate relative to uniform QAM signaling, by accounting for non-uniform reliabilities of each constellation distorted through screen-camera channels.

Related Works and Our Contributions: The studies on screen-camera communications can be divided into high-speed and reliable short-range communications and simultaneous screen-to-camera and screen-to-eye communications. In former studies, PixNet [13] is a pioneer work of high-speed and reliable communications for screen-camera links. PixNet employs frequency-domain grayscale transmission based on an orthogonal discrete multi-tone (DMT) scheme so that data distortion will be less sensitive against distance-dependent pixel mixing and blurring. However, since the original PixNet doe not fully exploit color attributes, the achievable throughput is still limited. In addition, DMT requires a relatively high-

complexity Fourier transform. For low-complexity smartphone applications, COlor Barcode stReaming for smArtphones (CO-BRA) [15] designed a two-dimensional (2D) color barcode. Each pixel within the barcode assigns one of four colors, i.e., red, green, blue, and white, to transmit two bits. For decoding, the receiver restores the pixel color values using hue saturation value (HSV) color model. Strata [16] hierarchically encodes transmission data to increase the capacity and spatial detail with multiple layers. In Smartphone Visible Light Communication (SVLC) [35], the sender divides transmission data into multiple small cells, and the same intensity is assigned to pixels within the same cell. At the receiver, the received cells are quantized based on the received pixel value distribution within the cell for denoising.

In the latter studies, they realize concurrent screen-to-camera and screen-to-eye communications. For example, Hi-Light [36] conveys data bits through the pixel transparency change within a time window. InFrame++ [4] leverages the capability discrepancy and distinctive features between human vision system and camera devices. They use spatial-temporal complementary frames (STCFs) to carry data bits without impairing user's viewing experiences.

Our study mainly focuses on the former studies. Our scheme aims to improve throughput for short range applications, e.g., near field communication and augmented reality by using precoding techniques at the sender's device. Although these techniques have been discussed in wireless and optical communications, there are no discussion and evaluations on impacts of such techniques for high-speed screen-camera communications. This is because screen-camera link is typically uni-directional and it requires another communication scheme, e.g., Wi-Fi, to exchange the estimated channel gains between the sender and the receiver. On the other hand, the recent off-the-shelf receivers, e.g., mobile phones and wearable cameras, have a radio communication module to exchange information between the sender via a radio channel. For the case of screen-camera communications between two mobile phones, it is also natural to consider bi-directional screen-camera communications as recent smart phones are equipped with both screens and cameras. For such systems having feedback medium, one of issues in precoding-based screen-camera communications is the amount of overhead for channel feedback. From the experimental evaluations, linear and nonlinear precodings realize better throughput at short and long communication distances under a negligible feedback overhead. We note that the frequency-domain equalization techniques can be introduced for simultaneous screen-to-camera and screen-to-eye communications to improve bit error rates by reducing nonlinear channel distortion.

II. Screen-Camera Visual MIMO Communications

A. System Overview

The purpose of our study is to achieve higher transmission rate in screen-camera communications. Fig. 1 shows the schematic of our proposed scheme. We use a pair of screen and camera as the sender and receiver, respectively. Note that there are three major differences from RF wireless communications.
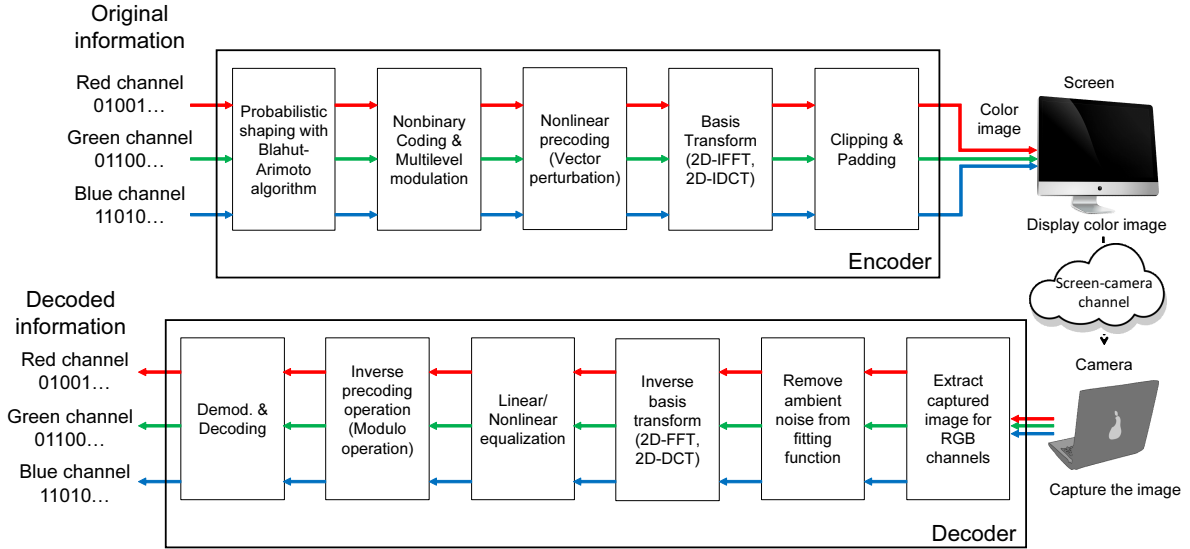
Fig. 1. Sender and receiver operation in screen-camera visual MIMO communications.

First, input values for the screen, i.e., pixel luminance values, should not be complex-valued numbers. Second, the input values are two dimensional (2D) in spatial domain. Third, the pixel luminance values typically range over finite non-negative integers, i.e., $0, 1, \ldots, 255$ for 8-bit quantization.

Based on the constraints, the sender first encodes shaped original information with nonbinary coding, followed by 2^M-ary QAM format and nonlinear precoding, and arranges the modulated symbols into a 2D image matrix. The modulated coefficients are then transformed to pixel luminance values by taking inverse 2D fast Fourier transform (FFT) operation, and clipped according to the luminance range. Finally, padding is added to the 2D values prior to display. At the receiver side, pixel luminance values are captured by camera sensors and then extracts the transmitted region from the captured values using an edge detection algorithm. We also mitigate the effect of perspective distortion and ambient lights. Finally, the filtered pixel values are transformed to frequency components by 2D-FFT and equalized to obtain original information.

B. Sender

1) Basis Transform: In order to be robust against inter-pixel interference, we use a bases transform technique based on 2D-FFT. The stream of QAM-modulated symbols are transformed to pixel luminance values using inverse 2D-FFT for each color channel. As mentioned above, the screen only accepts real values as the input luminance. To ensure output values from inverse 2D-FFT are purely real, we arrange the 2D matrix to be Hermitian symmetry. Note that the output from inverse FFT will be entirely real when the input values are Hermitian.

More specifically, we suppose the use of screen image having a resolution of $H \times W$ pixels for each color channel, for transmitting $3HW$ real values in total over three color channels. For each color channel, modulated QAM symbols are arranged into a matrix of size $H \times (W/2)$ and the 1D inverse FFT is carried out for each column. The FFT coefficients are

organized to be Hermitian symmetry by assigning the complex conjugate of the value at the (i, j)th frequency coefficient to the $(i, -j)$th frequency coefficient. The coefficients in each row are then fed into inverse FFT. The resulting HW values are all real and can be sent as screen image. As an alternative basis function, we also investigate discrete cosine transform (DCT), which may be suited for real-valued data transform.

2) Clipping: We consider 8 bits for quantization representation of pixel luminance for screen images. To ensure the output of FFT being within the range between 0 and 255, the pixel luminance values are shifted and scaled to have a mean of $255/2$ and a variance of $(255/2c_{\text{tail}})^2$, where c_{tail} is a clipping parameter. All values outside the range between 0 and 255 are clipped to 0 and 255, respectively. When the FFT size is large enough, the luminance values may follow a Gaussian distribution according to the central limit theorem. By adjusting the clipping parameter c_{tail}, we can control the probability of clipping events. For example, 99.99% of luminance values before clipping may lie within the 8-bit integer range for $c_{\text{tail}} = 4$.

3) Padding: Since light emitted from an LCD screen is diffusive in nature, each photo detector of camera sensors receives multiple lights from nearby LCD pixels. As a result, the LCD pixels are blended into one camera pixel in particular for long distance and mobile devices due to blur. The FFT-based transmission is insensitive to linear inter-pixel interference induced by the blur. However, this blending effect can still cause performance degradation at edges of the screen images, i.e., background values outside the encoded pixels can interfere. To reduce the edge effect, pixels with white color are appended around the encoded values as padding. Finally, the encoded values with padding are displayed on the screen with black background. Note that the white padding is also useful for edge detection at the receiver.
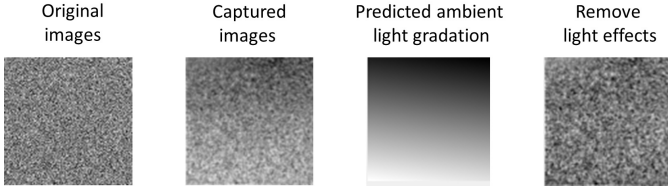
Fig. 2. An example of ambient light correction. A captured image is distorted due to ambient lights. Our scheme calculates the ambient noise by a least-squares fitting function and subtracts the noise from the captured image.

C. Receiver

1) Data Extraction: Receiver's camera first captures an image, which contains the transmitter's screen, for communications. Prior to decoding, the area of encoded pixels is extracted from the captured image. This requires the receiver to detect the four corners of the area. In our implementation, the encoded values can be extracted by detecting edges between white padding and black background based on [37].

2) Perspective and Ambient Light Correction: The extracted image is typically trapezoid and its luminance is shifted due to perspective distortion and ambient light distortion. We correct the perspective distortion by using homography operation [38]. Specifically, a trapezoid image can be transformed to a rectangle image based on four corners of images.

The proposed scheme then reduces the noise of ambient lights from the rectangle image. We recall the mean of encoded pixel values is shifted to $255/2$ at the transmitter, and thus shall align the mean of pixel luminance values of the rectangle image to zero before demodulation. To this end, our scheme subtracts the pixel values by the output of a best-fit linear function of $f(p_i, p_j) = ap_i + bp_j + c$ by means of least-squares method, where p_i and p_j are vertical index and horizontal index for pixels, respectively.

Fig. 2 shows an example of ambient light correction. As shown in the captured image, the luminance is brighter than the original luminance due to the ambient lights. Based on the output of a fitting function, the receiver estimates the noise from ambient lights and then subtracts the noise from the captured image to reduce impairments.

3) Decoding: The filtered luminance values are then fed into 2D-FFT and equalized to mitigate impairments due to screen-camera channels. After the receiver uses standard 2^M-ary QAM demodulation to calculate log-likelihood ratio (LLR), the channel decoding is carried out for the LLR values to obtain original information.

D. Linear/Nonlinear Equalization

In screen-camera communications, transmitted symbols are impaired by color mixing and an effective noise in frequency domain, e.g., due to motion blur. Let $\mathbf{y}_{i,j}$ denote a 3×1 vector of received symbols at (i, j)th frequency component. Each entry represents received symbols from red, green, and blue color channels, respectively. We assume that the received symbols are modeled as nonlinear systems:

$$\mathbf{y}_{i,j} = \mathbf{H}_{i,j}\phi(\mathbf{x}_{i,j}) + \mathbf{z}_{i,j}, \tag{1}$$

where $\mathbf{x}_{i,j}$ is a 3×1 vector of transmitted symbols in frequency domain, $\mathbf{H}_{i,j}$ is a $3 \times K$ channel gain matrix, $\mathbf{z}_{i,j}$ is a 3×1 additive white Gaussian noise (AWGN) vector with a noise variance of $\sigma_{i,j}^2$. Here, $\phi(\cdot)$ denotes a nonlinear kernel expansion and K is an expansion cardinality. For example, the second-order Volterra series expansion (including an offset term) [19]–[21] is expressed as $\phi(\mathbf{x}) = [1, \mathbf{x}^T, \mathbf{x}^T \otimes \mathbf{x}^T]^T$ with $K = 1 + 3 + 3^2 = 13$. Here, $\otimes$ represents Kronecker product and $[\cdot]^T$ is a transpose.

Rather than using maximum-likelihood equalization for $\phi(\mathbf{x}_{i,j})$ with expanded channel estimation, we employ MMSE equalization for the Volterra series expansion of the received symbols, i.e., $\phi(\mathbf{y}_{i,j})$. Specifically, MMSE filter weights of size $3 \times K$ are obtained as follows:

$$\mathbf{G}_{i,j} = \mathbb{E}\big[\mathbf{x}_{i,j}\phi(\mathbf{y}_{i,j})^\dagger\big]\mathbb{E}\big[\phi(\mathbf{y}_{i,j})\phi(\mathbf{y}_{i,j})^\dagger\big]^{-1}, \tag{2}$$

where $\mathbb{E}[\cdot]$ and $[\cdot]^\dagger$ denote the expectation and Hermitian transpose, respectively. In practice, the expectation is taken place by averaging multiple measurements in the past. In this paper, we obtain the expectation from 90 measurements. In addition, we consider either first-order or second-order Volterra series expansion for $\phi(\cdot)$, respectively, as linear equalizer (LE) or nonlinear equalizer (NLE). We note that the decoding latency in LE and NLE was almost comparable in our implementation at the same modulation format. Finally, the received symbols are equalized using the MMSE filter as follows:

$$\hat{\mathbf{x}}_{i,j} = \mathbf{G}_{i,j}\phi(\mathbf{y}_{i,j}). \tag{3}$$

E. Nonbinary Channel Coding

To further improve the transmission rate, we use nonbinary channel coding [23]–[26] based on LDPC codes over Galois field of $\mathbb{GF}(Q)$ [23] for 2^M-ary QAM transmissions. Although a number of practical communications systems have used binary coding in a context of bit-interleaved coded modulation (BICM) [39], theoretical gap from Shannon limit cannot be negligible. In particular, higher-order modulation does not always provide higher throughput when BICM is used. To compensate for the loss, we may consider BICM with iterative decoding (BICM-ID) [40] or multilevel coding (MLC) [41]. However, those methods may increase the decoding latency because of the feedback nature. In contrast, the nonbinary coded-modulation can resolve the performance and latency drawbacks for arbitrary order of modulation formats by allowing increase of decoding complexity.

For the Galois field size of $Q = 2^M$, a sender encodes every M-bit tuple of original data by using the Q-ary LDPC code. The encoded bits are sequentially mapped to symbol constellations with 2^M-ary modulation schemes. At the receiver side, the received symbols are demodulated to calculate an LLR vector $[L_0, L_1, \ldots, L_{Q-1}]$. The qth LLR value is expressed as

$$L_q = \ln \frac{\Pr(\hat{x}|b = 0)}{\Pr(\hat{x}|b = q)}, \tag{4}$$

where $\Pr(\hat{x}|b = q)$ denotes the likelihood:

$$\Pr(\hat{x}|b = q) \propto \exp\Big(-\frac{1}{\sigma_q^2}|\hat{x} - \chi_q|^2\Big), \tag{5}$$

i.e., the probability that the equalized signal is $\hat{x}$ conditioned on the transmitted symbol χ_q, the qth QAM constellation, where an effective noise variance after equalization is denoted by σ_q^2. The LLR vector is fed into a nonbinary LDPC decoder based on FFT Q-ary sum-product algorithm (QSPA). We consider a hypothetical decoder to estimate achievable throughput.

F. Precoding

When a sender has a knowledge of channel condition based on receiver's feedback, the sender can use precoding for transmission rate improvement. Each transmission symbol is precoded based on the channel gain matrix $\mathbf{H}_{i,j}$ as follows:

$$\mathbf{x}'_{i,j} = \mathbf{H}_{i,j}^+ \mathbf{x}_{i,j} = \mathbf{H}_{i,j}^\dagger \left(\mathbf{H}_{i,j} \mathbf{H}_{i,j}^\dagger + \kappa \mathbf{I} \right)^{-1} \mathbf{x}_{i,j}, \quad (6)$$

where $\mathbf{H}_{i,j}^+$ is a regularized pseudo inverse of $\mathbf{H}_{i,j}$ with κ being a regularization parameter, $\mathbf{x}'_{i,j}$ is the precoded transmission symbol, and $\mathbf{I}$ is an identity matrix of appropriate size. Although the precoding can resolve the color mixing prior to transmission, the drawback of the channel-inversion precoding includes a power increase of transmission signals $\mathbf{x}'_{i,j}$, which can exceed the 8-bit representation of pixel luminance. In order to reduce the amplitude of the symbol $\mathbf{x}'_{i,j}$, we also consider nonlinear precoding based on VP [28]–[30].

VP uses a lattice perturbation vector to reduce power enhancement due to the channel inversion. Specifically, the precoded transmission symbol $\mathbf{x}'_{i,j}$ can be obtained as follows:

$$\mathbf{x}'_{i,j} = \mathbf{H}_{i,j}^+ \left(\mathbf{x}_{i,j} + \tau \mathbf{d}_{i,j} \right), \quad (7)$$

where τ is a scalar value for VP, and $\mathbf{d}_{i,j}$ is 3×1 integer vector over the lattice points $\mathbb{Z}$. In order to limit the signal amplitude, we select the best lattice point, which minimizes the signal power via sphere decoding as follows:

$$\mathbf{d}_{i,j} = \arg\min_{\hat{\mathbf{d}} \in \mathbb{Z}} \left\| \mathbf{H}_{i,j}^+ \left(\mathbf{x}_{i,j} + \tau \hat{\mathbf{d}} \right) \right\|^2. \quad (8)$$

At the receiver side, the lattice perturbation can be removed from the equalized symbols by the modulo operation:

$$\hat{\hat{\boldsymbol{x}}}_{i,j} = \hat{\mathbf{x}}_{i,j} \bmod \tau, \quad (9)$$

which wraps the signal $\hat{\mathbf{x}}_{i,j}$ within a region from $-\tau$ to τ in each quadrature component-wise.

G. Probabilistic Shaping

Let $\mathbf{p} = [p_0, p_1, ..., p_{2^M-1}]$ denote the shaping vector, where p_q is the probability that the constellation χ_q is chosen for shaped transmission. To optimize $\mathbf{p}$ achieving the maximum transmission rates, we employ a generalized version of Blahut–Arimoto algorithm (BAA) [42], in which the following recursion is taken place until convergence:

$$p_q = \frac{p_q \exp[\bar{w} D_q(\mathbf{p})/w_q]}{\sum_i p_i \exp[\bar{w} D_i(\mathbf{p})/w_i]}, \quad (10)$$

where $\bar{w} = \min_i w_i$ and w_q is a conditional weight. Typically, we use $w_q = |\chi_q|^2$ for maximizing the mutual information

Fig. 3. Experimental equipment.

conditioned on the average signal energy $\sum_q p_q |\chi_q|^2$. Here, $D_q(\mathbf{p})$ is the relative entropy defined as

$$D_q(\mathbf{p}) = \int \Pr(\hat{x}|b=q) \ln \frac{\Pr(\hat{x}|b=q)}{\sum_{j=0}^{Q-1} p_j \Pr(\hat{x}|b=j)} \mathrm{d}\hat{x}, \quad (11)$$

where the integration over $\hat{x}$ is replaced with a discrete-output sum over a number of proximal sample points. For screen-camera communications, we use $w_q = 1$ for all q because peak-to-average power ratio is more important than average signal power. Note that the conventional probabilistic shaping generally considers homogeneous channel outputs, where the effective noise variance is identical over different constellation points. Nevertheless, the above BAA can take the nonuniform noise variance σ_q^2 for different q in (5) into consideration.

According to the optimized probability $\mathbf{p}$ obtained via BAA, we can generate non-uniform constellations by geometric Huffman coding [43]. Note that the LLR calculation for LDPC decoding should account for the shaping probability when probabilistic shaping is used; specifically, (4) is modified as

$$L_q = \ln \frac{\Pr(\hat{x}|b=0)p_0}{\Pr(\hat{x}|b=q)p_q}. \quad (12)$$

H. Computational Complexity

The processing time for frequency-domain approaches is dominated by the 2D-FFT according to [15], which demonstrated that the conventional PixNet can operate up to 100 frame-per-second (FPS) to send grayscale images of size 800×480 pixels using 1 GHz processor at Nexus S smartphone. Our scheme requires at least 3-times more FFT operations for color images, in addition to extra operations including nonbinary decoding and channel equalization. The FFT-QSPA complexity for nonbinary LDPC decoding is $\mathcal{O}[Q/\log_2 Q]$-times higher than binary counterparts. For example of $Q = 8$ to be used for 64QAM, the complexity is at most 2.7-fold increased. The computational complexity for the channel equalization is $\mathcal{O}[3KHW]$ for matrix multiplication in (3), where the weight matrix in (2) can be adaptively computed on a few occasions. As the computational complexity for color 2D-FFT is $\mathcal{O}[3HW \log_2 HW]$, the channel equalization

TABLE I
OPTIMIZED c_{tail} VALUES OVER COMMUNICATION DISTANCE

Modulation	60 cm	80 cm	100 cm	120 cm	140 cm	160 cm
4-QAM	2	1	1	2	1	2
16-QAM	2	2	2	2	1	1
64-QAM	2	2	1	3	2	1

is less time-consuming than FFT in general ($K = 3$ for linear equalization). For a moderate size of images, e.g., $H = W = 100$, the total complexity of the proposed method is roughly 4-fold higher than the conventional grayscale PixNet. Hence, we believe that our method is still feasible for practical mobile computing. With a careful choice of image sizes and recent smartphones, it is highly expected that the proposed scheme can operate at a high FPS such as 120.

III. PERFORMANCE EVALUATIONS

A. Experimental Methodology

We use IODATA EX-LD3151DB with a resolution of 1920×1080 as a display screen. We also use MacBook Pro 13-inch with 1080×720 resolution camera, iPad Air 2 with 960×960 resolution camera, and ZenPad 3 8.0 with 1600×900 resolution camera as an image sensor camera as shown in Fig. 10. To display encoded values on the screen, we use Psychophysics Toolbox Version 3 [44], which is a free set of Matlab functions with a precise control of display timing.

We evaluate the achievable throughput of the screen-camera communications system in terms of bits per frame. The throughput is defined as follows.

$$R = B \cdot \mathcal{I}(X; Y), \qquad (13)$$

where R denotes throughput (bits/frame), B is the total number of transmitted bits in one encoded image, and $\mathcal{I}(X; Y)$ is mutual information between a transmitted image X and equalized image Y. Here, the mutual information for nonbinary coding is calculated from the LLR vector as follows:

$$\mathcal{I}(X; Y) = \mathcal{H}_Q(\mathbf{p}) - \mathbb{E}\left[\log_Q\left(\sum_{q=0}^{Q-1} \exp(-L_q)\right) \middle| b = 0\right], \qquad (14)$$

where $\mathcal{H}_Q(\mathbf{p})$ is the Q-ary entropy function for nonuniform probability $\mathbf{p}$, defined as

$$\mathcal{H}_Q(\mathbf{p}) = -\sum_{q=0}^{Q-1} p_q \log_Q(p_q). \qquad (15)$$

When binary coding is considered, the mutual information is obtained analogously with $Q = 2$. Note that the nonuniform probability degrades the entropy for $\mathcal{H}_Q(\cdot)$, whereas the total mutual information $\mathcal{I}(X; Y)$ can be improved by BAA.

Unless otherwise stated, we evaluate the achievable throughput at a distance between the screen and camera of 60 cm. We also make an analysis of the throughput for different distances of 80, 100, 120, 140, and 160 cm. We use 90 images with a resolution of $H \times W = 100 \times 100$ for communications. Each image is displayed at the center position of the LCD screen. For clipping parameters of c_{tail} in each image, we use the
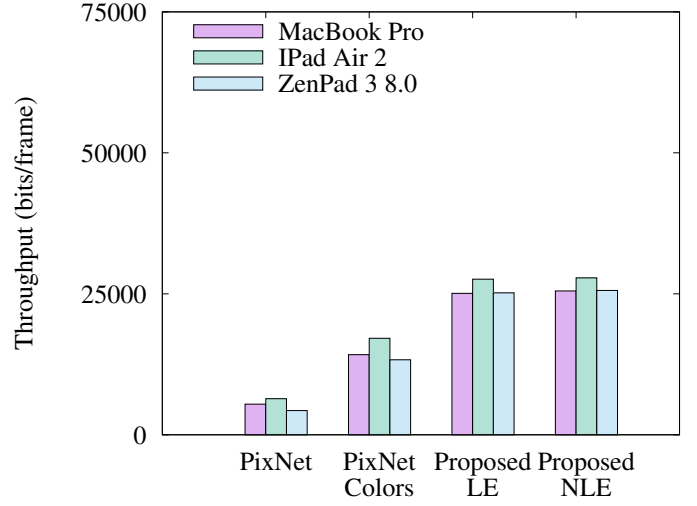

Fig. 4. Throughput of reference schemes with 4-QAM at a distance of 60 cm using different image sensor cameras: PixNet uses binary LDPC codes, while the proposed scheme uses nonbinary LDPC codes.

best values in different conditions obtained from preliminary experiments. Table I lists the best clipping parameters of c_{tail} in each modulation format and communication distance.

B. Baseline Performance

In Fig. 4, we show the performance of screen-camera links using three cameras, i.e., MacBook Pro, iPad Air 2, and ZenPad 3 8.0, for four reference schemes: PixNet [13], PixNet with color channels, proposed scheme with linear equalization, and proposed scheme with nonlinear equalization. All the reference schemes use 4-QAM for the modulation format at a communication distance of 60 cm in Fig. 4. PixNet uses the binary LDPC code for channel coding, and encoded values are displayed on green color channel for simplicity. The other schemes use red, green, and blue color channels. The proposed schemes use the nonbinary LDPC code for channel coding.

From Fig. 4, we can observe the following two points:

- The proposed scheme with NLE achieves the highest throughput.
- Even without NLE, our scheme realizes higher performance compared to the existing PixNet schemes because color mixing can be mitigated by LE.

For example, the throughput of our scheme with NLE using MacBook Pro is 4.5 times higher than PixNet and 1.8 times higher than PixNet with color channels. It suggests that equalization techniques are more advantageous for high-speed screen-camera communications.

In addition, it is demonstrated that the equalization techniques can be improved the throughput irrespective of camera quality. For example, the throughput of our scheme with NLE is 1.6 and 1.9 times higher than PixNet with color channels when we use iPad Air 2 and ZenPad 3 8.0 as an image sensor camera, respectively. It is thus expected that the proposed scheme can yield high throughput with even lower-end cameras. Since the achievable throughput of the proposed
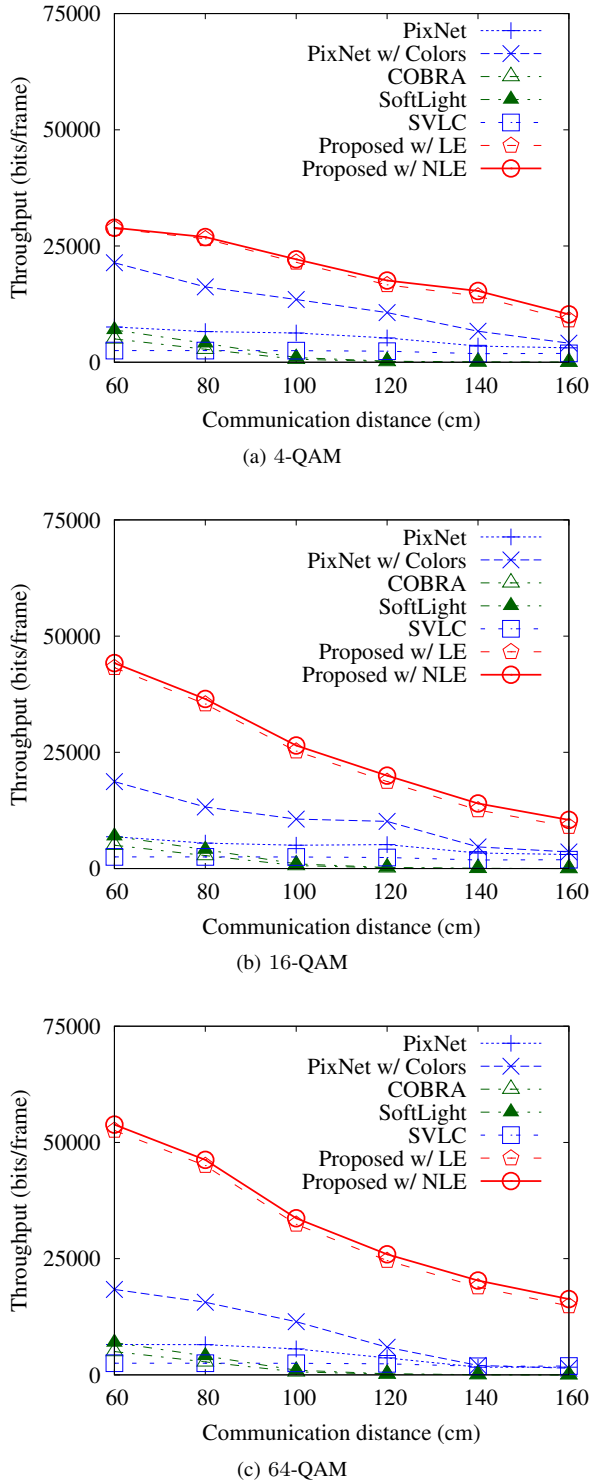
Fig. 5. Throughput as a function of communication distances.

we shall use higher-order modulation schemes to increase the throughput. To evaluate the impact of the distance and high-order modulation in throughput, we compare the achievable throughput with 16-QAM and 64-QAM at a distance of 80, 100, 120, 140, or 160 cm in addition to 4-QAM and 60 cm.

Figs. 5 (a) through 5 (c) show the throughput with 4-QAM, 16-QAM, and 64-QAM as a function of communication distance, respectively. Even in a longer distance, the proposed scheme keeps a higher throughput compared to the conventional schemes irrespective of modulation schemes. For instance, the proposed scheme with 4-QAM achieves 3.3 times higher throughput than PixNet and 2.5 times higher throughput than PixNet with color channels at a communication distance of 160 cm. It is also seen that PixNet without color channels is more robust than PixNet with color channels; specifically, color channels do not provide 3 times higher throughput in longer distance regimes. Since the intensity of blue color channel is weaker than other color channels, throughput of the color channel decreases in long-range communications.

In view of modulation schemes, high-order modulation boosts the performance improvement in the proposed schemes. On the other hand, high-order modulation schemes do not offer throughput improvement in the existing schemes because demodulation can fail without equalization. For example, the proposed scheme with 64-QAM yields 1.9 times higher throughput compared to the 4-QAM scheme at a communication distance of 60 cm. From these results, it is verified that high-order modulation schemes in conjunction with equalization techniques are effective for achieving high throughput. It is also observed that the nonlinear equalization can be more effective for higher-order modulation schemes although the performance improvement is marginal.

We then compare the performance of the proposed scheme with existing schemes of image-domain screen-camera communications, i.e., COBRA [15], SVLC [35], and SoftLight [17]. In COBRA, two bits per pixel are transmitted with a 2D color barcode and HSV model is used to decode the barcode. SoftLight is an improved version of COBRA by introducing bit-level rateless coding to realize rate-adaptive soft-decision decoding in the screen-camera communications.

Figs. 5 (a) through 5 (c) show the throughput results of COBRA, SoftLight, SVLC, PixNet, and the proposed scheme in different communication distances. Here, the size of each cell in SVLC is two. Since the existing schemes send the limited number of bits in each transmission image, they suffer lower throughput compared with the proposed scheme irrespective of the communication distances. In addition, the proposed scheme with a high-order modulation format yields better throughput by canceling linear and nonlinear effects using equalizations. In our experiments, SoftLight shows only a marginal improvement over COBRA because serious color/pixel-mixing occurs for pixel-domain barcodes. It suggests that our frequency-domain approach can send more data bits compared to the pixel-domain approaches over the whole range of communication distances in consideration.

In addition, we define a word error rate as an evaluation criterion to discuss the performance of our proposed scheme in terms of reliability. The error rate represents the number
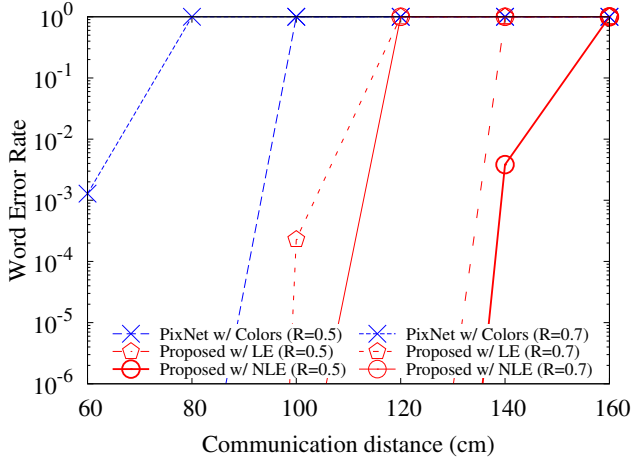
scheme is not sensitive to different cameras, we focus on iPad Air 2 as an image sensor camera in the following evaluations.

C. Impact of Distance and High-Order Modulation

Previous evaluations considered a fixed communication distance of 60 cm and modulation format of 4-QAM. However, when we use mobile devices for the communications, the distance between a sender and receiver may vary. In addition,

Fig. 6. Error rates in different communication distances for 4-QAM.

Fig. 7. Throughput with binary and nonbinary codes at a communication distance of 60 cm.

of erroneous codeword packets across the total number of transmitted packets. Fig. 6 shows error rates as a function of communication distances at a modulation format of 4-QAM in the proposed scheme and PixNet. Here, we assume irregular LDPC codes having a code rate of R and the code length of 512, which is relatively short so that high-throughput VLC is realized. By taking equalization techniques for the received signals, errors due to linear and nonlinear channel effects can be reduced and the error rate of the proposed scheme can be improved even in long communication distances. For example, the existing PixNet with color channels has a large error rate in a communication distance of 80 cm at a code rate of 0.5 while the proposed scheme with nonlinear equalization achieves a low error rate up to the communication distance of 120 cm. Note that the error rate results of other existing schemes were omitted to show because the word error rates were close to one for the whole range of distances at a code rate above 0.5.

D. Impact of Nonbinary Coding

This section discusses the contributions of nonbinary coding for performance improvement. In Fig. 7, we compare the throughput with binary and nonbinary codes, for 16-QAM and 64-QAM at a communication distance of 60 cm. It is demonstrated that the nonbinary coding offers performance improvement in particular for higher-order modulation with equalizations in our proposed scheme. Because BICM has a theoretical penalty, the throughput of 64-QAM can be lower than that of 16-QAM when binary coding is used.

Fig. 8 evaluates the throughput of the proposed scheme with binary and nonbinary codes as a function of communication distances. It shows that improvement by nonbinary codes can be obtained even in longer communication distances especially for higher-order modulation. For example, nonbinary code offers 2.1 times improvement on average across communication distances compared to the binary code scheme for 64-QAM. From these figures, it is highly recommended to integrate high-order modulation, nonbinary coding, and equalization for increasing the achievable throughput.
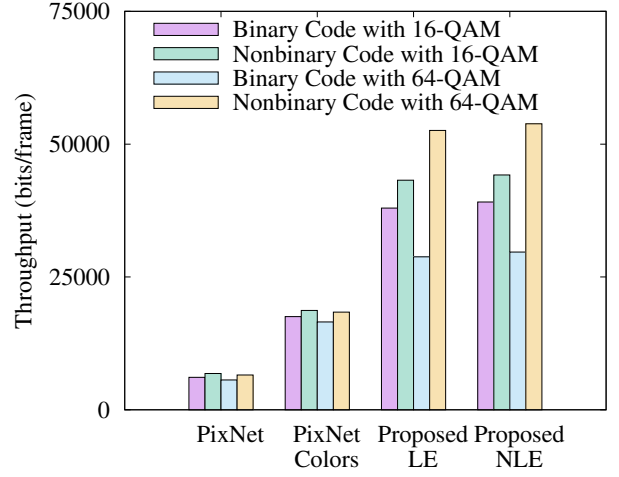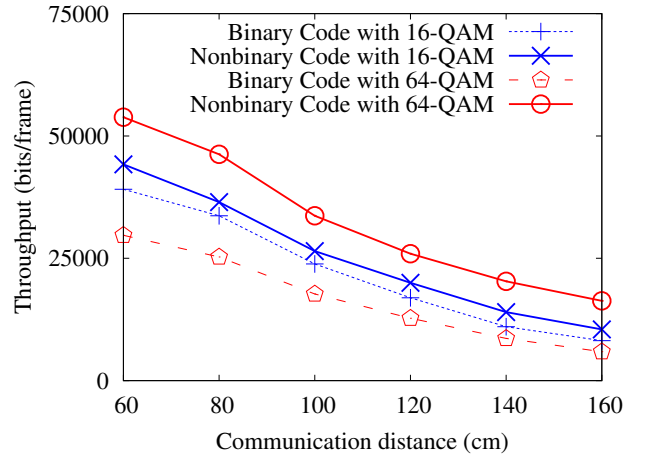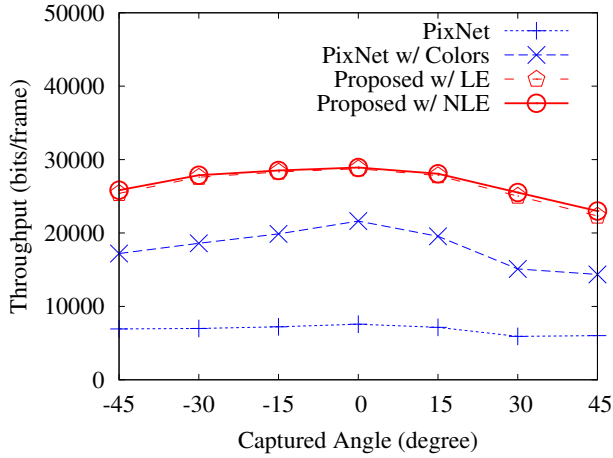

Fig. 8. Throughput of the proposed scheme with nonlinear equalization and binary/nonbinary codes as a function of communication distances.
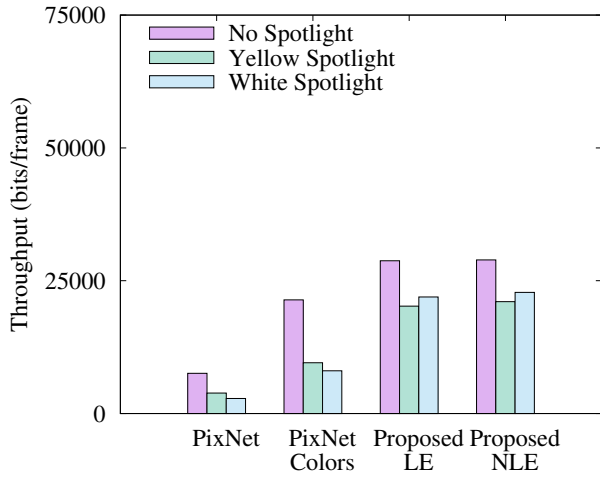
E. Effect of Different Conditions

In this section, we capture transmission images in different horizontal captured angles and spotlight colors to clarify the effectiveness of equalization techniques for various noise patterns in screen-camera communications.

Fig. 9(a) shows the throughput of the reference schemes as a function of the degree of horizontal captured angles at a communication distance of 60 cm and modulation format of 4-QAM. As the degree of captured angles increases, the throughput of each scheme decreases due to a strong perspective distortion. On the other hand, the proposed scheme keeps highest throughput throughout the captured angles by canceling the effects of perspective distortion.

In Fig. 9(b), we show the throughput results with different spotlight colors at a communication distance of 60 cm and modulation format of 4-QAM. Here, each captured image is distorted by yellow/white spotlight. In this case, some of captured pixel values are highly distorted by the spotlights. In PixNet with color channels, the throughput with yellow and

(a) Effects of angles

(b) Effects of spotlight colors

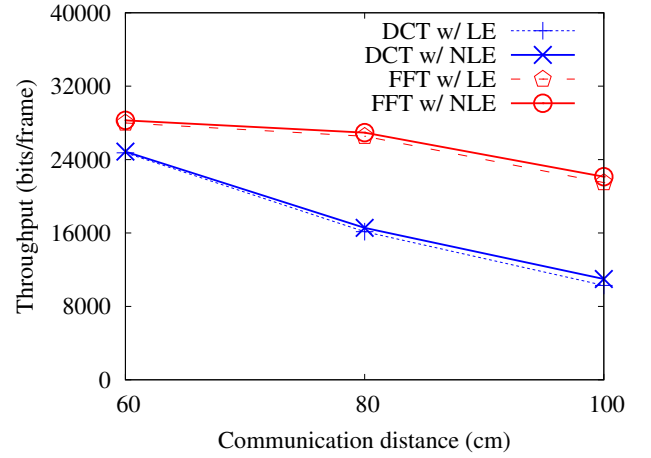Fig. 9. Throughput of reference schemes in different conditions.

Fig. 10. Throughput of the proposed scheme using FFT-based and DCT-based multiplexing.

DCT-based multiplexing decreases the throughput at a long communication distance. For example, the proposed scheme with FFT-based multiplexing offers 1.5 times improvement on average across communication distances compared to the DCT-based multiplexing.

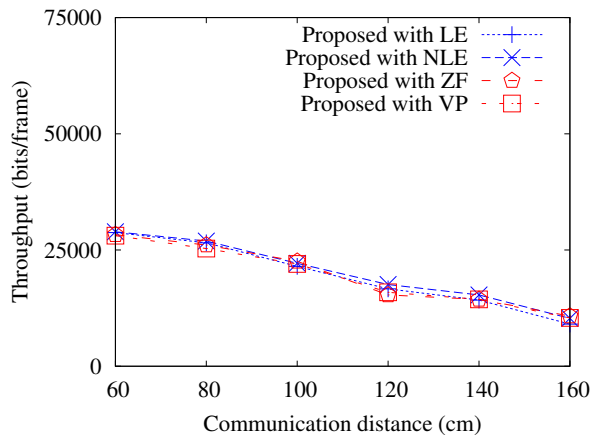### G. Impact of Linear/Nonlinear Precoding

This section considers linear precoding based on regularized zero-forcing (ZF) and nonlinear precoding based on VP to evaluate the impact in throughput performance on screen-camera links. For precoding, a receiver sends back estimated channel gains to a sender, and then the sender precodes transmission symbols based on the estimated channel gains to reduce the effect of channel impairments.
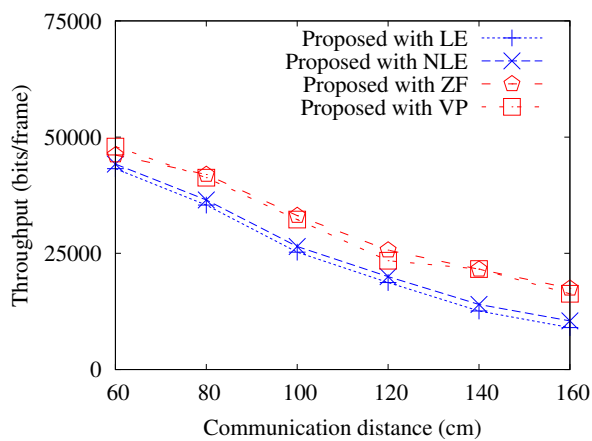
Figs. 11 (a) through 11 (c) show the throughput of the proposed scheme with/without linear and nonlinear precodings for different modulations. We note that both proposed with ZF and VP schemes use linear equalization at the receiver in addition to the precoding. From these results, we observe that linear and nonlinear precodings yield better performance in long communication distances. In addition, nonlinear precoding mostly performs better than linear precoding. The improvement comes from preventing noise boost by using perturbation vectors in nonlinear precoding.

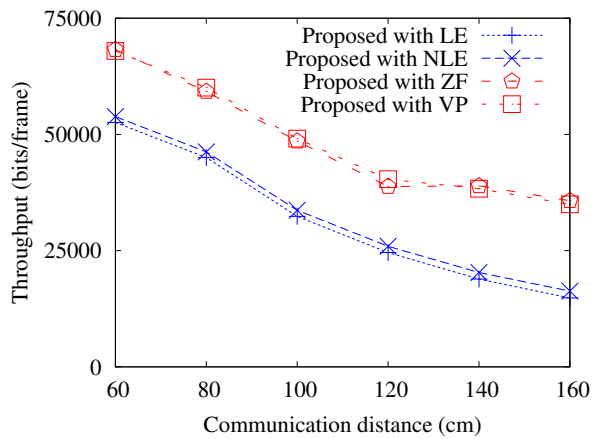### H. Impact of Probabilistic Shaping

Figs. 12 (a) and 12 (b) show that residual noise variance of each constellation point in blue color channel after nonlinear equalization. It was found that the variance σ_q^2 is non-identical for different q, specifically, the maximum variance is 2.6 and 3.7 times greater than the minimum variance in 16-QAM and 64-QAM, respectively. In this figure, we also present the probability p_q optimized by BAA, which can maximize the mutual information even in the presence of such nonuniform noise variances. To evaluate an impact of probabilistic shaping in screen-camera links, we evaluate throughput from simulations under the observed noise variances.

white spotlights is 55.3% and 62.4% lower than the throughput without spotlight, respectively. Although the throughput of the proposed scheme degrades due to spotlights, the effects of spotlight distortion can be marginal by using linear and nonlinear equalizations. For instance, the throughput degradation due to yellow and white spotlights is 27.2% and 21.1%, respectively, in our scheme with nonlinear equalization.

F. Impact of Basis Functions

Our scheme uses FFT-based multiplexing for transforming original information onto screen images. Here, we evaluate the impact of another basis transform, i.e., DCT, as an alternative of FFT. Note that imaginary parts of $H \times (W/2)$ QAM-modulated symbols are mapped to the rest of pixels to be real-valued images for DCT. For demultiplexing, an inverse 2D-DCT is taken place before displaying the pixel images.

In Fig. 10, we compare the throughput of the proposed scheme under the different multiplexing methods at a modulation format of 4-QAM. From this figure, it is seen that the proposed scheme with FFT-based multiplexing yields higher throughput than DCT-based multiplexing. Especially,
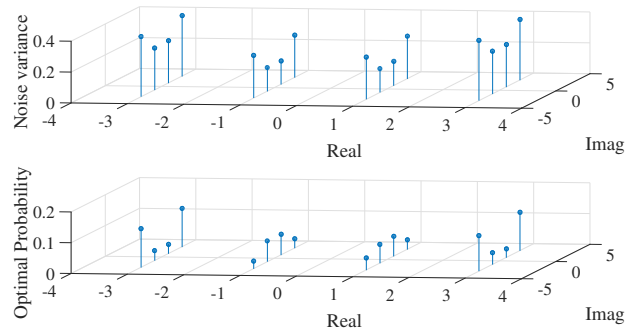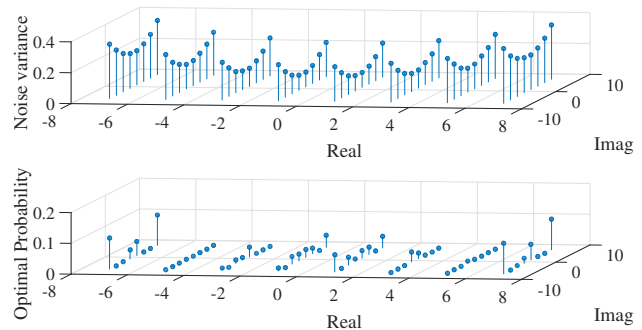
(a) 4-QAM

(b) 16-QAM

(c) 64-QAM

Fig. 11. Throughput of proposed schemes with ZF linear precoding and VP nonlinear precoding as a function of communication distances.

(a) 16-QAM

(b) 64-QAM

Fig. 12. Residual noise variance and shaping probability in each constellation point after nonlinear equalization at a communication distance of 60 cm.
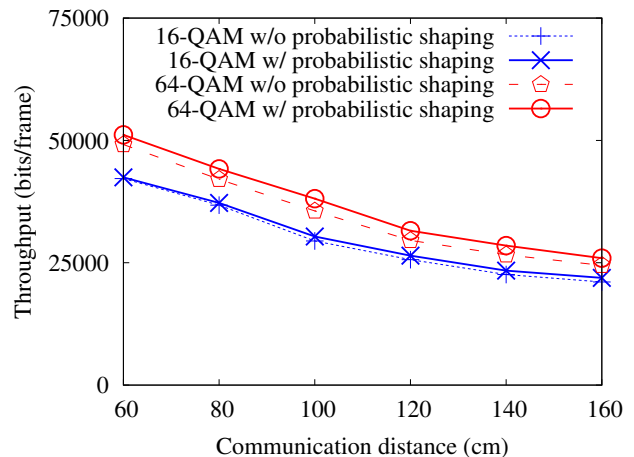

Fig. 13. Throughput of the proposed scheme with/without shaping.

Fig. 13 shows the throughput of the proposed scheme with/without probabilistic shaping in 16-QAM and 64-QAM as a function of the communication distance. It is shown that the probabilistic shaping can yield throughput improvement. For example, the proposed scheme with 64-QAM and probabilistic shaping offers 1,992 bits/frame higher throughput

compared to the proposed scheme without shaping on average across communication distances.

I. Discussion on Channel Feedback Interval

For nonlinear precoding at a sender, the receiver needs to send the estimated channel gains to the sender as a feedback. In this case, one of issues in precoding-based screen-camera communications is the amount of feedback overhead to be shared under a limited feedback occasion.
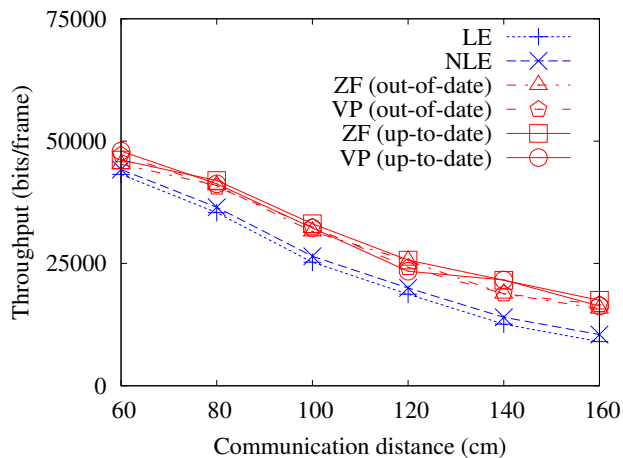
(a) 16-QAM

(b) 64-QAM

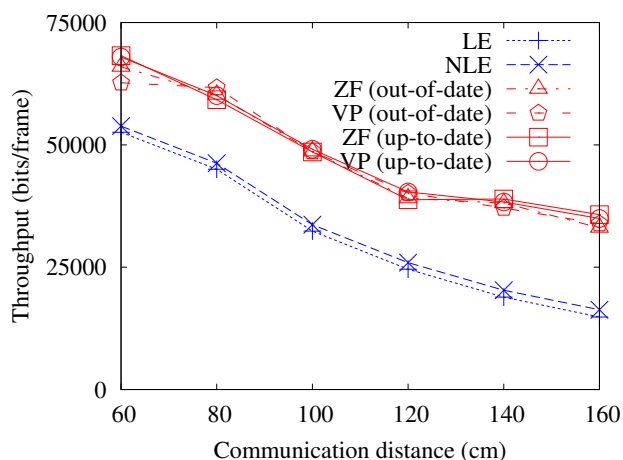Fig. 14. Throughput of proposed schemes with ZF linear precoding and VP nonlinear precoding using up-to-date and out-of-date channel information as a function of communication distances.

Fig. 14 shows the throughput of the proposed scheme using up-to-date and out-of-date feedback information to discuss an effect of the overhead. For delayed feedback updates, we consider tens-hours past feedback information for precoding. From experimental evaluations, precoding techniques can cancel the effects of screen-camera communication channel even when feedback interval is significantly long. It may suggest that the overhead requirement of the proposed scheme will be negligible for some cases where channel environment is stable.

IV. Conclusion

This paper proposed a new screen-camera communication scheme to improve the throughput of the visual MIMO links. To realize the improvement, our proposed scheme integrates color channels, high-order modulation, linear/nonlinear channel equalization, nonbinary coding, probabilistic shaping, and nonlinear precoding. We experimentally evaluated the achievable throughput of screen-camera communications, using a consumer-grade LCD screen and camera. Through the experiments, we demonstrated that the proposed scheme achieves 3.3

times higher throughput than conventional schemes. We also demonstrated that our scheme keeps higher throughput than the existing schemes for longer communication distances between the screen and camera by reducing channel impairments. To the best of our knowledge, this is the first experimental demonstration exploiting channel equalization, nonbinary coding, probabilistic shaping, and nonlinear precoding for screen-camera communications in the literature.

References

[1] H. Burchardt, N. Serafimovski, D. Tsonev, S. Videv, and H. Haas, "VLC: Beyond point-to-point communication," *IEEE Communications Magazine*, vol. 52, no. 7, pp. 98–105, 2014.

[2] P. H. Pathak, X. Feng, P. Hu, and P. Mohapatra, "Visible light communication, networking and sensing: A survey, potential and challenges," *IEEE Communications Surveys & Tutorials*, vol. 17, no. 4, pp. 2047–2077, 2015.

[3] E. Curry, D. Borah, and J. M. Hinojo, "Optimal symbol set design for generalized spatial modulations in MIMO VLC systems," in *IEEE GLOBECOM*, 2016, pp. 1–7.

[4] A. Wang, Z. Li, C. Peng, G. Fang, and B. Zeng, "InFrame++: Achieve simultaneous screen-human viewing and hidden screen-camera communication," in *ACM MobiSys*, 2015, pp. 181–195.

[5] R. LiKamWa, D. Ramirez, and J. Holloway, "Styrofoam: A tightly packed coding scheme for camera-based visible light communication," in *ACM MobiCom workshop on Visible light communication systems*, 2014, pp. 27–32.

[6] V. Nguyen, Y. Tang, A. Ashok, M. Gruteser, K. Dana, W. Hu, and E. Wengrowski, "High-rate flicker-free screen-camera communication with spatially adaptive embedding," in *IEEE INFOCOM*, 2016, pp. 1–9.

[7] M. Izz, Z. Li, H. Liu, Y. Chen, and F. Li, "Uber-in-light: Unobtrusive visible light communication leveraging complementary color channel," in *IEEE INFOCOM*, 2016, pp. 1–9.

[8] T. Yamazato, I. Takai, H. Okasa, T. Fujii, T. Yendo, S. Arai, M. Andoh, T. Harada, K. Yasutomi, K. Kagawa, and S. Kawahito, "Image-sensor-based visible light communication for automotive applications," *IEEE Communication Magazine*, vol. 52, no. 7, pp. 88–97, 2014.

[9] A. Wang, S. Ma, C. Hu, J. Huai, C. Peng, and G. Shen, "Enhancing reliability to boost the throughput over screen-camera links," in *ACM Annual International Conference on Mobile Computing and Networking*, 2014, pp. 41–52.

[10] W. Hu, H. Gu, and Q. Pu, "Lightsync: Unsynchronized visual communication over screen-camera links," in *ACM Annual International Conference on Mobile Computing and Networking*, 2013, pp. 15–26.

[11] T. W. Kan, C. H. Teng, and W. S. Chou, "Applying QR code in augmented reality applications," in *ACM International Conference on Virtual Reality Continuum and its Applications in Industry*, 2009, pp. 253–257.

[12] A. Ashok, S. Jain, M. Gruteser, N. Mandayam, W. Yuan, and K. Dana, "Capacity of pervasive camera based communication under perspective distortions," in *IEEE International Conference on Pervasive Computing and Communications*, 2014, pp. 114–120.

[13] S. Perli, N. Ahmad, and D. Katabi, "Pixnet: Interference-free wireless links using LCD-camera pairs," in *ACM Annual International Conference on Mobile Computing and Networking*, 2010, pp. 137–148.

[14] W. Huang, C. Gong, P. Tian, and Z. Xu, "Experimental demonstration of high-order modulation for optical camera communication," in *IEEE Symposium on Signal Processing for Optical Wireless Communications*, 2015, pp. 1027–1031.

[15] T. Hao, R. Zhou, and G. Xing, "COBRA: Color barcode streaming for smartphone systems," in *ACM International Conference on Mobile Systems, Applications, and Services*, 2012, pp. 85–98.

[16] W. Hu, J. Mao, Z. Huang, Y. Xue, J. She, K. Bian, and G. Shen, "Strata: Layered coding for scalable visual communication," in *ACM Annual International Conference on Mobile Computing and Networking*, 2014, pp. 79–90.

[17] W. Du, J. C. Liando, and M. Li, "SoftLight: Adaptive visible light communication over screen-camera links," in *IEEE Annual conference on Computer Communications*, 2016, pp. 1–9.

[18] S. S. Haykin, *Adaptive filter theory, 5th edition*. Pearson Education, 2013.

[19] M. Schetzen, *The Volterra and Wiener Theories of Nonlinear Systems*. Kriger, 1989.

[20] N. Mallouki, B. Nsiri, S. Mhatli, M. Ghanbarisabagah, W. Hakimi, M. Ammar, and E. Giacoumidis, "Analysis of full Volterra nonlinear equalizer for downlink LTE system," in *Wireless Telecommunications Symposium*, 2015, pp. 1–6.

[21] G. B. Giannakis and E. Serpedin, "Linear multichannel blind equalizers of nonlinear FIR Volterra channels," *IEEE Transactions on Signal Processing*, vol. 45, no. 1, pp. 67–81, 1997.

[22] S. Hranilovic and F. R. Kschischang, "A pixelated MIMO wireless optical communication system," *IEEE Journal of Selected Topics in Quantum Electronics*, vol. 12, no. 4, pp. 859–874, 2006.

[23] D. Declercq and M. Fossorier, "Decoding algorithms for nonbinary LDPC codes over GF," *IEEE Transactions on Communications*, vol. 55, no. 4, pp. 633–643, 2007.

[24] I. B. Djordjevic and B. Vasic, "Nonbinary LDPC codes for optical communication systems," *IEEE Photonics Technology Letters*, vol. 17, no. 10, pp. 2224–2226, 2005.

[25] S. Pfletschinger, A. Mourad, E. Lopez, D. Declercq, and G. Bacci, "Performance evaluation of non-binary LDPC codes on wireless channels," in *ICT Mobile and Wireless Communications Summit*, 2009.

[26] M. Arabbaci, I. B. Djordjevic, R. Saunders, and R. M. Marcoccia, "High-rate nonbinary regular quasi-cyclic LDPC codes for optical communications," *Journal of Lightwave Technology*, vol. 27, no. 23, pp. 5261–5267, 2009.

[27] T. Koike-Akino, K. Sugihara, D. S. Millar, M. Pajovic, W. Matsumoto, A. Alvarado, R. Maher, D. Lavery, M. Paskov, K. Kojima *et al.*, "Experimental demonstration of nonbinary LDPC convolutional codes for DP-64QAM/256QAM," in *ECOC*, 2016, pp. 1–3.

[28] B. Hochwald, C. Peel, and L. Swindlehurst, "A vector-perturbation technique for near-capacity multi-antenna multi-user communication-part ii: Perturbation," *IEEE Transactions on Communications*, vol. 53, no. 3, pp. 537–544, 2005.

[29] E. Casaneda, A. Silva, A. Gameiro, and M. Kountouris, "An overview on resource allocation techniques for multi-user MIMO systems," *IEEE Communications Surveys & Tutorials*, vol. PP, no. 99, pp. 1–45, 2016.

[30] M. M. Sebdani, W. Krzymien, and J. Melzer, "Massive MIMO with nonlinear precoding: Large-system analysis," *IEEE Transactions on Vehicular Technology*, vol. 65, no. 4, pp. 2815–2820, 2016.

[31] M. Yankov, D. Zibar, K. Larsen, and L. Christensen, "Constellation shaping for fiber-optic channels with QAM and high spectral efficiency," *IEEE Photonics Technology Letters*, vol. 26, no. 23, pp. 2407–2411, 2014.

[32] T. Fehenberger, D. Lavery, R. Maher, A. Alvarado, P. Bayvel, and N. Hanik, *Sensitivity Gains by Mismatched Probabilistic Shaping for Optical Communication Systems*. IEEE Photonics Technology Letters, 2016, vol. 28, no. 7.

[33] L. Szczecinski and A. Alvarado, *Bit-Interleaved Coded Modulation: Fundamentals, Analysis and Design*. John Wiley & Sons, 2015.

[34] T. Fujihashi, T. Koike-Akino, P. Orlik, and T. Watanabe, "Experimental throughput analysis in screen-camera visual MIMO communications," in *IEEE GLOBECOM*, 2016, pp. 1–6.

[35] R. Boubezari, H. L. Minh, Z. Ghasemlooy, and A. Bouridane, "Smartphone camera based visible light communication," *Journal of Lightwave Technology*, vol. 34, no. 17, pp. 4120–4126, 2016.

[36] T. Li, C. An, X. Xiao, A. T. Campbell, and X. Zhou, "Real-time screen-camera communication bihind any scene," in *ACM MobiSys*, 2015, pp. 1–15.

[37] T. Muppirala, "Video sudoku solver," 2016. [Online]. Available: https://jp.mathworks.com/matlabcentral/fileexchange/30088-video-sudoku-solver

[38] E. Vincent and R. Laganiere, "Detecting planar homographies in an image pair," in *International Symposium on Image and Signal Processing and Analysis*, 2001, pp. 1–6.

[39] G. Caire, G. Taricco, and E. Biglieri, "Bit-interleaved coded modulation," *IEEE Transactions on Information Theory*, vol. 44, no. 3, pp. 927–946, 1998.

[40] X. Li and J. A. Ritcey, "Bit-interleaved coded modulation with iterative decoding using soft feedback," *Electronics Letters*, vol. 34, no. 10, pp. 942–943, 1998.

[41] U. Wachsmann, R. F. Fischer, and J. B. Huber, "Multilevel codes: Theoretical concepts and practical design rules," *IEEE Transactions on Information Theory*, vol. 45, no. 5, pp. 1361–1391, 1999.

[42] M. Jimbo and K. Kunisawa, "An iteration method for calculating the relative capacity," *Information and Control*, vol. 43, no. 2, pp. 216–223, 1979.

[43] G. Böchererand and R. Mathar, "Matching dyadic distributions to channels," in *Proc. Data Compression Conf.*, 2011.

[44] D. H. Brainard, "The psychophysics toolbox," in *Spatial Vision 10*, 2016, pp. 433–436.

Takuya Fujihashi (M'16) received Ph.D. degree from the Graduate School of Information Science and Technology, Osaka University, Japan, in 2016. He is currently an assistant professor at the Graduate School of Science and Engineering, Ehime University since Jan. 2017. He was research fellow (PD) of Japan Society for the Promotion of Science in 2016. From 2014 to 2016, he was research fellow (DC1) of Japan Society for the Promotion of Science. From 2014 to 2015, he was an intern at Mitsubishi Electric Research Labs. (MERL) working with the Electronics and Communications group. He selected one of the Best Paper candidates in IEEE ICME (International Conference on Multimedia and Expo) 2012. His research interests are in the area of video compression and communications, with a focus on multi-view video coding and transmission over high and low quality networks.

Toshiaki Koike-Akino (M'05–SM'11) received the B.S. degree in electrical and electronics engineering, M.S. and Ph.D. degrees in communications and computer engineering from Kyoto University, Kyoto, Japan, in 2002, 2003, and 2005, respectively. During 2006–2010, he was a Postdoctoral Research Fellow at Harvard University, and joined Mitsubishi Electric Research Laboratories, Cambridge, MA, USA in 2010. His research interest includes signal processing for data communications, sensing, and machine learning. He received the YRP Encouragement Award 2005, the 21st TELECOM System Technology Award, the 2008 Ericsson Young Scientist Award, the IEEE GLOBECOM'08 Best Paper Award in Wireless Communications Symposium, the 24th TELECOM System Technology Encouragement Award, and the IEEE GLOBECOM'09 Best Paper Award in Wireless Communications Symposium.

Philip V. Orlik (S'97–M'99) was born in New York, NY in 1972. He received the B.E. degree in 1994 and the M.S. degree in 1997 both from the State University of New York at Stony Brook. In 1999 he earned his Ph.D. in electrical engineering also from SUNY Stony Brook. In 2000 he joined Mitsubishi Electric Research Laboratories located in Cambridge, MA, where he is currently the Group Manager of the Electronics&Communications Group. His primary research focus is on advanced wireless and mobile communications, sensor networks, ad hoc networking and UWB. Other research interests include vehicular/car-to-car communications, mobility modeling, performance analysis, and queuing theory.

Takashi Watanabe (S'83–M'87) is a Professor of Graduate School of Information Science and Technology, Osaka University, Japan. He received his B.E. M.E. and Ph.D. degrees from Osaka University, Japan, in 1982, 1984 and 1987, respectively. He joined Faculty of Engineering, Tokushima University as an assistant professor in 1987 and moved to Faculty of Engineering, Shizuoka University in 1990. He was a visiting researcher at University of California, Irvine from 1995 through 1996. He has served on many program committees for networking conferences, IEEE, ACM, IPSJ, IEICE (The Institute of Electronics, Information and Communication Engineers, Japan). His research interests include mobile networking, ad hoc networks, sensor networks, ubiquitous networks, intelligent transport systems, specially MAC and routing. He is a member of IEEE, IEEE Communications Society, IEEE Computer Society as well as IPSJ and IEICE.